Proceedings of the ASME/JSME 2011 8^{th} Thermal Engineering Joint Conference
AJTEC2011
March 13-17, 2011, Honolulu, Hawaii, USA

AJTEC2011-44664

DETAILED NUMERICAL MODELING OF A MICROCHANNEL REACTOR FOR METHANE-STEAM REFORMING

Kevin Drost
School of Mechanical, Industrial and Manufacturing Engineering
Oregon State University
Corvallis, Oregon 97331
Email: drostk@onid.oregonstate.edu

Benn Eilers
School of Mechanical, Industrial and Manufacturing Engineering
Oregon State University
Corvallis, Oregon 97331
Email: eilersb@onid.orst.edu

Daniel Peterson
School of Mechanical, Industrial and Manufacturing Engineering
Oregon State University
Corvallis, Oregon 97331
Email: dpeterso@engr.orst.edu

Sourabh V. Apte
School of Mechanical, Industrial and Manufacturing Engineering
Oregon State University
Corvallis, Oregon 97331
Email: sva@engr.orst.edu

Vinod Narayanan
School of Mechanical, Industrial and Manufacturing Engineering
Oregon State University
Corvallis, Oregon 97331
Email: vinod.narayanan@oregonstate.edu

John Schmitt
School of Mechanical, Industrial and Manufacturing Engineering
Oregon State University
Corvallis, Oregon 97331
Email: schmitjo@engr.orst.edu

ABSTRACT

Numerical modeling of methane-steam reforming is performed in a microchannel with heat input through Palladium-deposited channel walls corresponding to the experimental setup of Eilers [1]. The low-Mach number, variable density Navier-Stokes equations together with multicomponent reactions are solved using a parallel numerical framework. Methane-steam reforming is modeled by three reduced-order reactions occurring on the reactor walls. The surface reactions in the presence of Palladium catalyst are modeled as Neumann boundary conditions to the governing equations. Use of microchannels with deposited layer of Palladium catalyst gives rise to a non-uniform distribution of active reaction sites. The surface reaction rates, based on Arrhenius type model and obtained from literature on packed-bed reactors, are modified by a correction factor to account for these effects. The reaction-rate correction factor is obtained by making use of the experimental data for specific flow conditions. The modified reaction rates are then used to predict hydrogen production in a microchannel configuration at different flow rates and results are validated to show good agreement. It is found that the endothermic reactions occurring on the catalyst surface dominate the exothermic water-gas-shift reaction. It is also observed that the methane-to-steam conversion occurs rapidly in the first half of the mircochannel. A simple one-dimensional model solving steady state species mass fraction, energy, and overall conservation of mass equations is developed and verified against the full DNS study to show good agreement.

NOMENCLATURE

A Pre-exponential constant, $[kmol/m^2 - s]$
A_c Cross sectional area of the physical plant, $[m^2]$
C_i Concentration of the i^{th} chemical species, $[kmol_i/m^3]$
c_p Specific heat, $[kJ/kg - K]$
$\mathscr{D}_{i,m}$ Binary diffusion coefficient, i corespondents to the chemical species, $[m^2/s]$
$E_{a,k}$ Activation energy of the k^{th} reaction, $[kJ/mol]$
h Specific enthalpy of mixture, $[kJ/kg]$
$h^o_{f_i}$ Specific enthalpy of formation of the i^{th} species, $[kJ/kg]$

ΔH^0_{298} Specific heat of reaction at reference temperature $298K$, $[kJ/mol]$
$\Delta H_{R,k}$ Specific heat of reaction of the k^{th} reaction, $[kJ/mol]$
k Thermal conductivity of mixture, $[kW/m-K]$
k_f Specific reaction rate constant,$[kmol/m^2-s]$
$\mathscr{M}_i$ Molecular weight of species i, $[kg_i/kmol_i]$
N_s Number of chemical species
n Wall normal direction
p Pressure, $[Pa]$
q_j Heat flux due to conduction and species diffusion, $[kW/m^3]$
$\dot{Q}_{total}$ Flow rate of both inlet methane and steam, $[ml/min]$
r_k Reaction rate of k^{th} reaction, $[kmol/m^2-s]$
$\dot{s}_i$ Rate of chemical species adsorption and desorption at the catalyst surface of species i, $[kmol_i/m^2-s]$
R Universal gas constant, $[kJ/kmol-K]$
t Time, $[s]$
T Absolute temperature, $[K]$
u_i Velocity in tensor notation where $i=1,2,3$ corespondents to the x, y and z directions, $[m/s]$
$\overline{u}$ Mean velocity in the x direction, $[m/s]$
x_i Direction of the i^{th} directions, $[m]$
Y_i Species mass fraction of species i, $[kg_i/kg_{mixture}]$
$Y_{bulk,i}$ Bulk species mass fraction of species i, $[kg_i/kg_{mixture}]$
α Temperature exponent, $[1]$
μ Viscosity of mixture, $[kg/m-s]$
ν''_{ki} Stoichiometric coefficient of the i^{th} chemical species in reaction k of reactants, $[1]$
ν'_{ki} Stoichiometric coefficient of the i^{th} chemical species in reaction k of products, $[1]$
Φ_v Viscous dissipation, $[N/m^2-s]$
ρ Density of mixture, $[kg/m^3]$
$\dot{\omega}'''_i$ Reaction rate of the k^{th} reaction, $[mol_i/m^2-s]$

INTRODUCTION

The present work investigates conversion efficiency of biomass-based gaseous products (CH_4,CO_2) using a microchannel reactor. This design exploits the short diffusion lengths for reactant gases in microchannels, such that the reaction may occur near stoichiometric conditions (using very less excess reactant gases), thereby substantially increasing the efficiency of the system. Such a design has several advantages: (a) reduced mixing time for non-premixed reactants since diffusion time is limited by the cross-section of microchannels, (b) very high heat transfer rates in microchannels, and (c) damage to one of the microchannels does not cause catastrophic failure of the reactor.

The main motivation behind this study is to investigate technological feasibility of *solar thermochemical* processing, wherein the heat input to the microchannel reactor will be obtained by designing a solar receiver/reactor that can concentrate the incident solar energy flux onto the microchannel walls. It is envisioned that the solar receiver will be a cylindrical cavity wherein the incident heat flux will be distributed along the interior walls of the cavity. Several, parallel microchannels can be arranged around the periphery of such a receiver, with heat flux input through the bottom wall. One such microchannel is considered in the present fundamental study to understand issues relevant to hydrogen production from methane-steam reforming. Note that heat loss issues can be prevented in such receivers by insulating the receiver.

In order to study the technical feasibility of such a design, we first investigate, through numerical simulations, the strong endothermic reactions of methane-steam reforming inside a microchannel reactor with *Palladium* catalyst. The low-Mach number, unsteady, variable-density Navier-Stokes equations together with species mass-fraction and energy equations are solved in a microchannel. The surface chemical reactions are modeled as boundary conditions to the energy and species equations for a reduced reaction mechanism of methane-steam reforming [2, 3, 3–5]:

$$CH_4 + H_2O \Longleftrightarrow CO + 3H_2; \quad \Delta H^0_{298} = +206 \text{ kJ/mol} \quad (1)$$
$$CO + H_2O \Longleftrightarrow CO_2 + H_2; \quad \Delta H^0_{298} = -41 \text{ kJ/mol} \quad (2)$$
$$CH_4 + 2H_2O \Longleftrightarrow CO_2 + 4H_2; \quad \Delta H^0_{298} = +165 \text{ kJ/mol}. \quad (3)$$

There have been several studies on microchannels reactors with Rhodium, Palladium or Nickel catalysts arranged in the form of a packed bed [4–7]. Recently, Wang *et. al.* [3] investigated the effects of steam-methane inlet ratio and flow rates on hydrogen production, in a planar solid-oxide fuel cells (SOFC) using experimental and numerical modeling in steady-state. Kuznetsov & Kozlov [2] investigated, using numerical simulations, the effect of heat flux distribution on methane-steam reforming using reduced reaction mechanisms in a microchannel with Nickel catalyst.

The primary goal of this work is to first validate the numerical model based on solution to conservation equations of mass, momentum, and energy coupled with surface chemical kinetics against the experimental data by co-workers [1]. Specifically, for microchannel configurations, deposition of catalyst on the surface can result in non-uniform distribution providing intermittent active sites for chemical reaction. Without detailed quantification of these active sites, their effect on the production of H_2 cannot be modeled. In the present work, a *reaction-rate correction factor* is introduced wherein the pre-exponential factor in reaction rates for surface chemical kinetics is modified by a constant to account for active site distribution. In order to obtain this correction factor, experimental data from one of the flow tests is used. The constant is calibrated to match the exit hydrogen molar concentrations. This reaction-rate correction factor is then kept fixed and several other flow conditions are computed to validate the predicted hydrogen levels at the exit. With such validation,

detailed information inside the microchannel reactor, that is not available in experiments, is obtained.

The second goal of this work is to investigate the effect of inlet steam-methane ratio, the distribution of surface wall temperature or external heat flux on the species diffusion, physicochemical reactions and heat transfer processes inside the microchannel reactor. A simple one-dimensional model solving steady state species mass fraction, energy, and overall conservation of mass equations is developed and verified against the full DNS study to show good agreement. Work is ongoing in relation to these parametric variations.

The paper is arranged as follows. The mathematical formulation and reaction rate kinetics are summarized first. A brief description of the numerical approach is given next. The flow geometry, validation studies, and results based on experimental configuration of Eilers [1] are presented next followed by summary and conclusions.

MATHEMATICAL FORMULATION

The mathematical formulation is based on the variable-density, Navier-Stokes equations together with species mass-fraction and enthalpy equations [8]:

$$\frac{\partial \rho}{\partial t} + \frac{\partial}{\partial x_j}(\rho u_j) = 0; \tag{4}$$

$$\frac{\partial \rho u_i}{\partial t} + \frac{\partial}{\partial x_j}(\rho u_i u_j) = -\frac{\partial p}{\partial x_i} + \frac{\partial \tau_{ij}}{\partial x_j}; \tag{5}$$

$$\frac{\partial \rho Y_i}{\partial t} + \frac{\partial}{\partial x_j}(\rho u_j Y_i) = \frac{\partial}{\partial x_j}\left(\rho \mathscr{D}_{i,m} \frac{\partial Y_i}{\partial x_j}\right) + \dot{\omega}_i'''; \ \mathrm{i} = 1...\mathrm{N_s} \tag{6}$$

$$\frac{\partial \rho h}{\partial t} + \frac{\partial}{\partial x_j}(\rho u_j h) = -\frac{\partial q_j}{\partial x_j} + \mu \Phi_v; \tag{7}$$

where N_s, ρ, u_i, Y_i, p, h, q_j, and Φ_v represent the number of species transport equations, density, velocity components, species mass fraction, pressure, total enthalpy, heat flux due to conduction and species diffusion, and viscous dissipation, respectively. The mixture is assumed as an ideal gas with the viscosity, thermal conductivity, and the binary diffusion coefficient ($\mathscr{D}_{i,m}$) depending upon the local composition and temperature. The mixture density is obtained from the equation of state for an ideal gas,

$$p = \frac{\rho RT}{\mathscr{M}_{mixture}}, \tag{8}$$

where, R is the universal gas constant, p is the operating pressure, and T is the mixture temperature. The mixture molecular weight is given by the expression, $\mathscr{M}_{mixture} = (\sum_i^{N_s} \frac{Y_i}{\mathscr{M}_i})^{-1}$, where N_s is the total number of species.

The gas-phase reaction rates ($\dot{\omega}_i'''$) are functions of temperature, species concentration, and pressure field [6, 7]. The total enthalpy h is given as

$$h = h^o_{f_{mix}} + \int_{T_{ref}}^{T} c_{p_{mix}} dT; \quad h^o_{f_{mix}} = \sum_i^{N_s} Y_i h^o_{f_i}. \tag{9}$$

Where, h is the total enthalpy of the mixture, $h^o_{f_{mix}}$ is the enthalpy of formation of the mixture, $h^o_{f_i}$ is the enthalpy of formation for the i^{th} species, $c_{p_{mix}}$ is the specific heat of the mixture (the mass weighted average of the species' specific heat), N_s is the total number of species and T_{ref} is a reference temperature.

Chemical Kinetics and Surface Reactions

In the microchannel-based solar reactor, chemical reactions can occur in the gaseous phase as well as a series of reactions on the catalyst surface. Past studies by Deutschmann & Schmidt [6] on oxidation of steam in a tubular model showed that for atmospheric pressures, the gas-phase reactions contributed negligibly to the oxidation process; however, increase in reactor pressure beyond 10 bar resulted in sensitivity of the oxidation process to the gas-phase reactions. In the present work, we perform numerical experiments at atmospheric conditions and neglect the gas-phase reactions. The numerical solver presented in this work is, however, capable of accounting for the gaseous-phase chemical kinetics.

The catalytic reaction rates are nonlinear relations comprising the reactant species concentrations and the local temperature. Modeling of detailed chemical kinetics pathways for catalytic reactions on the surface have been performed [6, 9]; however, can become prohibitively expensive for time-resolved simulations performed in the present work. A reduced reaction mechanism with the following two endothermic (equations 1,3) and one exothermic water-gas shift (equation 2) global reactions was used to model the chemical conversion.

To calculate the reaction rates, the classical kinetic model was employed, wherein the reaction rates for each chemical reactions can be formulated as [10, 11],

$$r_k = k_{f,k} \Pi_{i=1}^{N_s} [\mathrm{C}_i]^{\nu'_{ki}}, \tag{10}$$

$$k_{f,k} = A_k \exp\left(-\frac{E_{a,k}}{RT}\right), \tag{11}$$

where C_i denotes the concentration per unit volume of the i^{th} chemical species in the mixture, $k_{f,k}$ is the specific reaction rate constant for the k^{th} reaction and ν'_{ki}, which is dimensionless, is the stoichiometric coefficient of the i^{th} chemical species in the k^{th} reaction. Experimental data for the reaction activation energy ($E_{a,k}$), the activation constants A_k and α_k for each k^{th} reaction is obtained from the experimental data [4, 5] for a specific catalyst.

The activation energy for the three reactions 1,2,3 are given as $E_{a,1} = 109.4$, $E_{a,2} = 15.4$ and $E_{a,3} = 209\,kJ/mol$, respectively [4, 5]. The pre-exponential factors for each reaction vary based on the catalyst type and are given for Nickel and Palladium catalysts in Table 1.

TABLE 1: Pre-exponential factors for the three reactions (equations 1,2,3) for Nickel and Palladium catalysts.

Catalyst	A_1	A_2	A_3
Nickel [4,5]	1.093×10^8	6.028×10^{-4}	5.922×10^3
Palladium [12]	89.6×10^9	543.5	371.1×10^9

It should be noted that the predictive capability of the numerical approach depends on accurate characterization of the surface reactions rates. Detailed chemical kinetics pathways for catalytic surface reactions [6, 9] were used in the modeling of the catalytic reaction on the channel surface. Kuznetsov and Koslov [2] used the same three-step reactions, however modeled the reaction rates using the expressions developed by Hou and Hughes [5], Xu and Froment [4] based on packed-bed reactor studies. In the present work,

In the present work, we are interested in microchannel configurations and use the above reaction rate models, owing to their Arrhenius-type standardized expressions. There have been previous studies on methane-steam reforming in minichannels [3] using similar three-step reduced reaction mechanism with Arrhenius-type reaction rates. As shown later, we first verify the applicability and predictive capability of the above model by simulating configurations corresponding to the work by Kuznetsov and Koslov [2] to show good comparisons between the two reaction-rate models.

With the above surface reaction rates, the catalytic conversion is then modeled simply through the following boundary conditions for the species mass-fractions and temperature equations [2, 6]:

$$-\rho \mathscr{D}_i \frac{\partial Y_i}{\partial n} = \dot{s}_i \mathscr{M}_i; \quad -k\frac{\partial T}{\partial n} = q_{wall} + \sum_k^3 r_k \Delta H_{R,k}, \qquad (12)$$

where $\dot{s}_i$ is the rate of chemical species adsorption and desorption at the catalyst surface, $\mathscr{M}_i$ is the molecular weight of species i, q_{wall} is the rate of external heat supplied to the wall, $\Delta H_{R,k}$ is the heat of reaction, r_k is the reaction rate of the k^{th} surface reaction. The surface adsorption and desorption rates depend on the coverage of the catalyst over the surface and surface site density [2, 6, 7]. In the present work, uniform catalyst surface density is assumed for the reactor conditions. The surface adsorption/desorption rates for each i^{th} species are obtained as:

$$\dot{s}_i = \sum_{k=1}^{3} \left(\nu'_{ki}(r_k) - \nu''_{ki}(r_k)\right), \qquad (13)$$

where the summation is over the three chemical reactions in the reduced reaction mechanism.

NUMERICAL IMPLEMENTATION

For the numerical implementation, it is assumed that the flow velocity is much smaller than the speed of sound and the mean thermodynamic pressure field within the microreactor remains approximately constant, such that the zero-Mach number assumption is valid. The numerical solver is based on a pressure-based, reacting flow solver on unstructured grids [13–16]. The flow solver has been used for two-phase reacting flow field in a realistic gas-turbine combustor and is able to capture the reaction dynamics in the microchannel configuration. The solver is three-dimensional, massively parallel and is suitable for large number of parameter variation studies.

The governing equations are solved using a fractional-step method. First, the scalar fields (the species concentrations and temperature fields) are solved in a conservative form using a third order WENO discretization [13, 16]. The new scalar fields are used to evaluate new mixture density using the ideal gas law. The momentum and continuity equations are solved using a pressure-based, predictor-corrector approach. The momentum equation is used to first predict a new velocity field. This velocity field is then corrected by solving a pressure-Poisson equation constraining the velocity field to satisfy the continuity constraint. The details of the numerical approach are given in [13,15,16].The total enthalpy equation is re-written in the form of a transport equation for the sensible enthalpy. This leads to a reaction source term based on the heats of formation of species in the gaseous phase. In the present work, gas-phase reactions are neglected. The catalytic surface reactions are modeled through boundary conditions for the gas-phase species.

NUMERICAL RESULTS

The numerical approach is first systematically verified and validated for a series of non-reacting and reacting flows in microchannel configurations. Specifically, we first verify our numerical approach together with the Arrhenius-type surface reaction rate model against the numerical studies on micrchannel methane-steam reforming performed by Kuznetsov and Koslov [2] using a Nickel catalyst. Their work uses the commonly used reaction rate model based on packed-bed reactor experiments by Hou and Hughes [5]. Once verified, we perform non-reacting and reacting flow configurations in the experimental

setup by co-workers [1] with Palladium catalyst. Here, the non-uniform distribution of active surface sites for catalytic reactions are accounted for by using a reaction-rate correction factor. The reaction rate correction factor is obtained by using experimental data for one particular flow condition. Different flow conditions are then simulated and predicted numerical results compared with the experimental data.

Non-reacting Flow in a Microchannel

Simple flow in a 3D channel, as studied by Qu *et al.* [17], serves as the initial test case. Validation of the flow solver for this test case is a critical step towards our simulation goal, since the parallel microchannel geometry of interest involves flow through microchannels with a high aspect ratio (see Fig. 1).

TABLE 2: Dimensions (in $[mm]$) for the single-microchannel [17].

Wch	Wp	Hch	Lp1	Lpch	Lp2
0.222	6.35	0.694	6.35	120	12.7

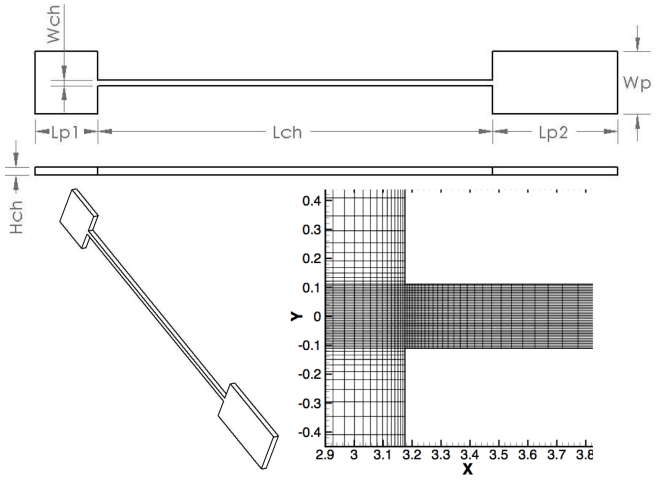

FIGURE 1: Schematic and grid for the single channel geometry. The grid used consists of around 1.5M grid elements. Only a small section of the grid is shown.

Channel dimensions are given in Table 2. As seen from the schematic, the ratio of plenum to microchannel height is very large. The computational grid consists of around 1.5 M grid points with roughly 30 cells inside the microchannel in the vertical direction. The grid cells are refined near the walls and near the entrance region to resolve the flow accurately. Fluid flow through the channel is simulated for different Reynolds numbers ($Re = 196$ and $Re = 1895$), and the resulting velocity profiles and pressure drops are compared with the experimental and numerical results presented in [17]. In these simulations, two large plenums are used at the inlet and outlet of the domain to ensure that the boundary conditions do not perturb the solution inside the channel. A fully developed velocity profile for a three-dimensional rectangular channel [17] is applied at the inlet of the domain and data is only collected after the flow in the channel reaches steady state.

Figure 2 illustrates the comparison of the simulated velocity profile over the cross-section at different locations within the channel to the numerical and experimental data of [17]. The simulations produce a parabolic profile and good agreement with the both the numerical and experimental results. For larger Reynolds numbers, the numerical velocity at the center of the channel is slightly larger than the experimental data; however, agrees with the simulations conducted by Qu *et al.* [17]. These deviations are within the uncertainties in maintaining constant flow rates as well as velocity measurements.

TABLE 3: Comparison between computed and theoretical pressure drops at different Reynolds numbers.

	Pressure Drop $[bar]$		
Re_{ch}	DNS (with plenum)	DNS without plenum)	Theory (without plenum)
196	0.189	0.195	0.20
1021	1.09	1.06	1.04
1895	1.33	1.87	1.93

Table 3 presents the comparison of numerically obtained pressure drop inside the microchannel with the theoretical pressure drop in a square microchannel (excluding the plenums). A good agreement is achieved for low Reynolds number (up to $Re_{ch} = 1021$). For $Re_{ch} = 1895$ the pressure drop is under-predicted by the simulation. This is attributed to the effects of sudden changes in aspect ratios near the inlet and outlet plenums. Flow separations are possible near the entrance, modifying the

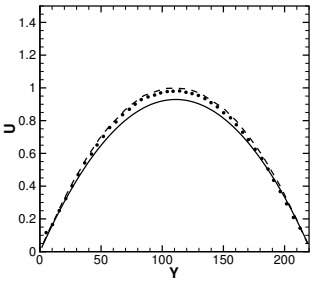

(a) $Re = 196, x' = 1\,cm$

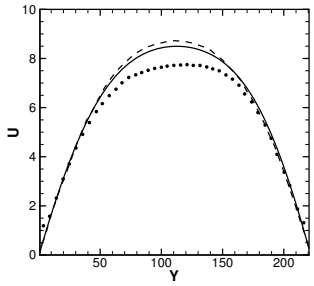

(b) $Re = 1895, x' = 1\,cm$

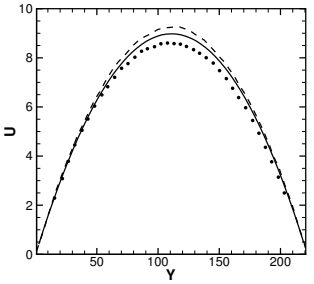

(c) $Re = 1895, x' = 10\,cm$

FIGURE 2: Velocity profiles in the center plane of the channel taken at $x' = 1\,cm$ and $x' = 10\,cm$ from the entrance of the channel. • shows the experimental data, $---$ the numerical simulation from [17] and — the present study. The velocity is expressed in $[m/s]$ and the y location in $[\mu m]$.

flow evolution to fully developed velocity profile and thus affecting the overall pressure drop. To test the accuracy of the solver, we have also simulated flow through the microchannel duct (without the plenums) with uniform inlet on a grid similar to the grid used for the case with plenums. The pressure-drop values for the same mass-flow rates are shown in Table 3 and agree well with the theoretical estimates.

Microchannel Methane-Steam Reforming with Nickel Catalyst

This study is performed to verify the accuracy of the Arrhenius-type reaction rate model (equation 11) for surface chemical reactions inside a microchannel with Nickel catalyst. Kuznetsov and Kolsov used a different reaction rate model as given below (from Hou and Hughes [5]):

$$r_1 = \frac{k_1 \left(\frac{P_{CH_4} P_{H_2O}^{0.5}}{P_{H_2}^{1.25}} \right) \left(1 - \frac{P_{CO} P_{H_2}^3}{K_{p1} P_{CH_4} P_{H_2O}} \right)}{\left(1 + K_{CO} P_{CO} + K_{H_2} P_{H_2}^{0.5} + K_{H_2O} \left(P_{H_2O} / P_{H_2} \right) \right)^2}, \quad (14)$$

$$r_2 = \frac{k_2 \left(\frac{P_{CO} P_{H_2O}^{0.5}}{P_{H_2}^{0.5}} \right) \left(1 - \frac{P_{CO_2} P_{H_2}}{K_{p2} P_{CO} P_{H_2O}} \right)}{\left(1 + K_{CO} P_{CO} + K_{H_2} P_{H_2}^{0.5} + K_{H_2O} \left(P_{H_2O} / P_{H_2} \right) \right)^2}, \quad (15)$$

$$r_3 = \frac{k_3 \left(\frac{P_{CH_4} P_{H_2O}}{P_{H_2}^{1.75}} \right) \left(1 - \frac{P_{CO_2} P_{H_2}^4}{K_{p3} P_{CH_4} P_{H_2O}^2} \right)}{\left(1 + K_{CO} P_{CO} + K_{H_2} P_{H_2}^{0.5} + K_{H_2O} \left(P_{H_2O} / P_{H_2} \right) \right)^2}. \quad (16)$$

This test case verifies the numerical approach for reacting flow with surface chemical kinetics modeling by comparing results with the numerical studies by Kuznetsov and Koslov [2].

Figure 3 shows a schematic of the computational domain with the height and spanwise length of $h = 0.5$ mm and $L = 112.5$ mm, respectively. A porous nickel catalyst section, on the top and bottom walls starts at flow length of 30 mm and continues up to the end of the channel. This catalyst configuration allows the flow to develop before the reaction zone. The Reynolds number varies between simulations but is always in the laminar flow regime. A structured Cartesian grid was used in this simulation with 25×800 control volumes in the vertical and axial directions, respectively. For the present study, variations in spanwise directions were assumed negligible, and a two-dimensional configuration is assumed. Simulations were performed for uniform, ramp-up and ramp-down variation of the heat flux input through the catalyst walls. The overall heat flux magnitude was kept constant at 2 kW/m^2. The average inlet velocity of the gas mixture is 0.67 m/s. Dirichlet conditions are specified for the species mass fraction, velocity and temperature at the inlet. Walls are modeled as no-slip and adiabatic, except the catalyst wall. For the catalyst wall, surface reactions are incorporated as boundary conditions given by expression 12. The exit boundary condition is implemented as a convective outflow.

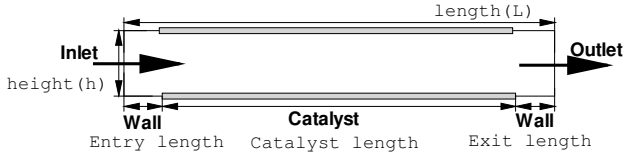

FIGURE 3: Schematic of the mini-channel reractor with catalyst on the top and bottom surfaces.

Figures 4 show the comparison of surface reaction rate profiles and the species mole fraction profiles along the length of the microchannel to the corresponding predictions by Kuznetsov and Koslov [2]. It is found that, the species molar fractions are well predicted by both approaches. Small deviations in the surface reaction rates are observed between the two models, however, their effect on the overall species or temperature distributions were minimal. It is also observed that the exothermic water-gas-shift reaction (reaction number 2 given by equation 2) has the smallest reaction rates compared to the other two endothermic reactions. This verifies the use of Arrhenius-type reaction rate model for microchannel-based configuration. Similar results were obtained for different heat flux profiles (not shown).

Microchannel Methane-Steam Reforming with Palladium Catalyst

Finally, we apply the numerical model to the microchannel setup corresponding to the work by co-authors [1]. Figure 5a shows the schematic of the setup. The initial two torches acted as preheaters for the reactor, whereas the subsequent seven torches impinged on the surface corresponding to the location of the catalyst and provided heat for the reaction. Half of the preheater zone had the same thermocouple arrangement as the catalyst zone, whereas in the other half the flame impinged directly on the reactor wall, thereby reducing heat transfer resistance. The Pd catalyst was contained on a porous FeCrAlY felt insert. The channel was held together with 30 8x32 stainless steel bolts distributed around the perimeter of the channel in order to distribute the compressive force as much as possible to minimize the potential for leaks in the system. To eliminate conduction between heating zones, 0.8 mm (1/32 in) air gaps separated each heating zone.

Non-Reacting Flow: The top section of the left pipe is 0.073 m long with a diameter of 0.0046 m the bottom section is 0.013 m long with a diameter of 0.0032 m the top section of the the right pipe is 0.061 m long with a diameter of 0.0046 m and the bottom section is 0.013 m long with a diameter of 0.0032 m. The height of the channel is 0.86 mm with a total length of 0.1735 m and a catalyst length of 0.133 m, the width of the channel is

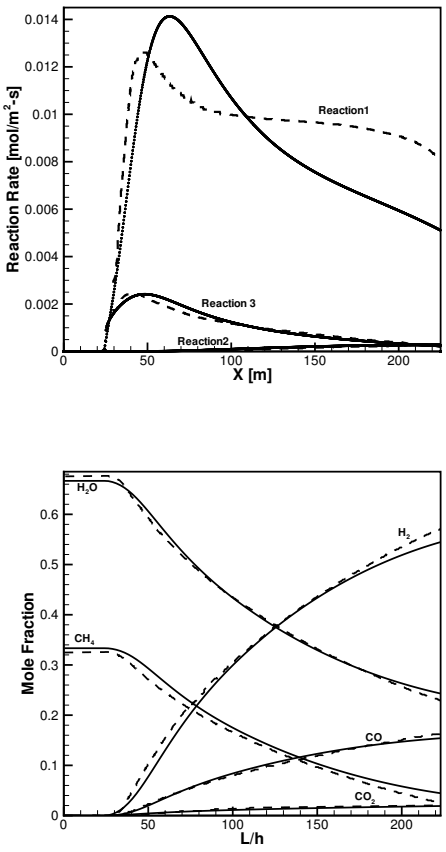

FIGURE 4: Reaction rate and species mole fraction profiles along the microchannel length for a uniform heat flux of 2 kW/m^2 though the catalyst walls: $(-)$ present, $--$ Kuznetsov and Koslov [2].

19 mm in the catalyst section (the section of the channel). A downward velocity at the inlet of the left pipe is enforced and an outflow condition on the end of the right pipe. All walls were given a no-slip condition. The inlet steam to methane ratio is 3.4.

First, for different flow rates, the pressure drop across the microchannel was computed and compared with the experimental data under non-reacting flow conditions. The pressure drop is measured between ends of the two circular pipes shown. Nitrogen gas was used as the acting fluid, this eliminates the reactions at the catalyst surface. Pressure drop was measured and modeled at different flow rates, the results of these pressure parametric study is shown in Figure 6. Good agreement is seen between the measured experimental pressure drop and the modeled numerical pressure drop.

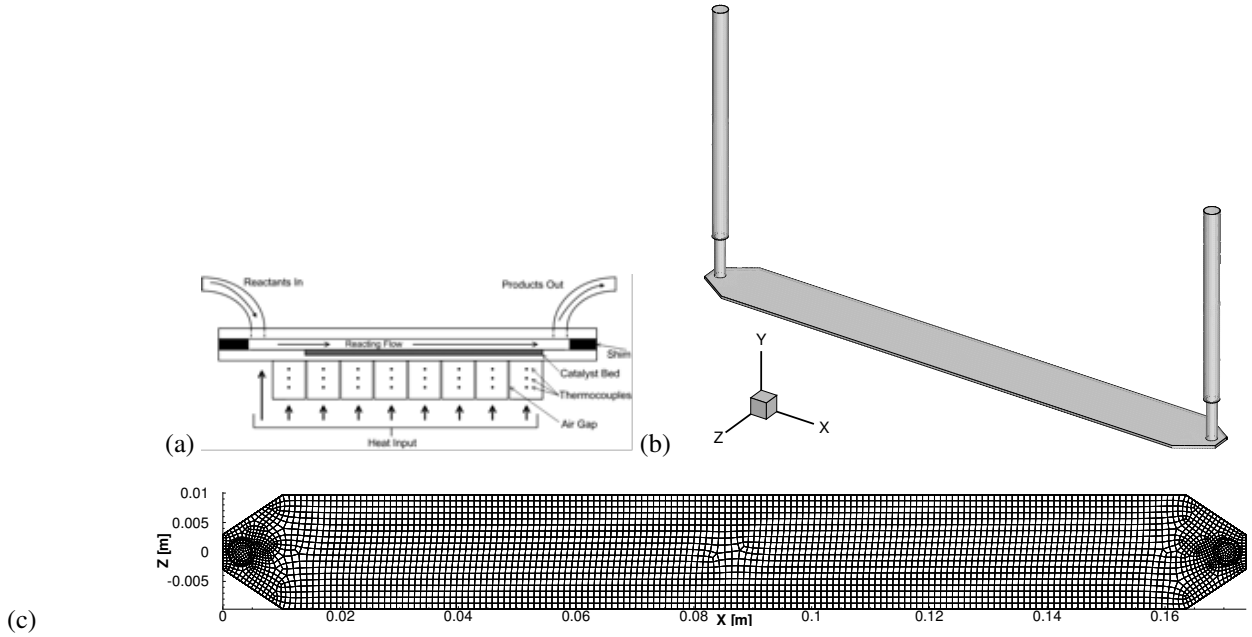

FIGURE 5: Experimental setup and numerical model: (a) schematic of experimental setup by Eilers [1], (b) the 3D flow model, (c) computational grid.

Reacting Flow: As mentioned earlier, the inlet methane-steam mixture is pre-heated by a pre-heat section (without wall catalyst). The catalyst used here was a porous felt with deposited palladium nanoparticles throughout the felt (chemical kinetics charactoristic are taken from Shu *et al.* [12]). For the case studied in this work (catalyst C), the channel wall was treated such that Palladium nanoparticles were deposited uniformly throughout the surface to give a porous catalyst bed. Figure 7 shows the SEM image of the catalyst bed after flow shearing test. For this test, one section was loaded into the reactor and exposed to a moderate temperature (500°C) high velocity (>10 m/s) flow of nitrogen to test for catalyst adhesion and durability (typical velocities during experiments were 5 m/s). Particle sizes on the order of 15 nm were observed but a large degree of agglomeration occurred as can be seen in figure 7. The nanoparticles can be seen as the clumped small round particles distributed throughout both figures. No noticeable reduction in particle density was observed after the shear testing, suggesting that particles were adequately adhered to the substrate.

As seen from the SEM image, it is clear that the active sites for surface chemical reactions are not uniformly distributed on the channel walls. In order to account for this distribution in the numerical model, it is necessary to quantify the surface distribution of the deposited Palladium catalyst. However, since the bed is porous, it is not straightforward to model its effect on the reaction rates. In the present work, we introduce a *reaction-rate correction factor*, α_s, that modifies the pre-exponential factor in the Arrhenius reaction rates (equation 10) as:

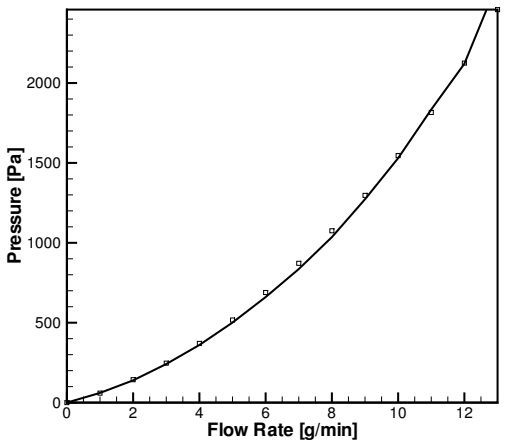

FIGURE 6: Comparison of pressure drops through the device at different flow rates: dashed line (−−) experiments [1], solid line (−) numerical.

$$k_{f,k} = \alpha_s A_k \exp\left(-\frac{E_{a,k}}{RT}\right). \quad (17)$$

The reaction-rate correction factor can be determined by us-

TABLE 4: Calibration studies to obtain reaction-rate correction factors by matching the exit hydrogen concentrations with experimental data [1].

Case	CH_4 Flow Rate g/min	H_2O:CH_4 Ratio	Inlet Velocity m/s	Inlet Temp. $^\circ C$	Heat Flux W/m^2	Computed α_s
C1	0.233	2.87	4.89	627	-154.8	0.0000101
C2	0.211	3.13	5.1	673.6	-7.727	0.0000184
C3	0.21	2.91	4.91	714	276.3	0.00004325
C4	0.203	2.96	5.09	761	399	0.0000612
C5	0.195	3.06	5.18	798.7	840.7	0.0000748
C6	0.188	3.25	5.38	836.9	1882	0.0001008
C7	0.183	2.87	5.06	902	3908	0.0001463

TABLE 5: Exit hydrogen concentration compared to experimental results for catalyst C [1] with a constant reaction rate correction factor of $\alpha_s = 6.6 \times 10^{-5}$.

Case	Methane Flow Rate g/min	Experiments H_2 Molar Fraction	Predicted H_2 Molar Fraction	Error
C3	0.21	0.0788	0.1066	35.28%
C4	0.203	0.1433	0.1488	3.84%
C5	0.195	0.219	0.2039	6.89%
C6	0.188	0.333	0.2831	14.98%
C7	0.183	0.4803	0.4068	15.30%

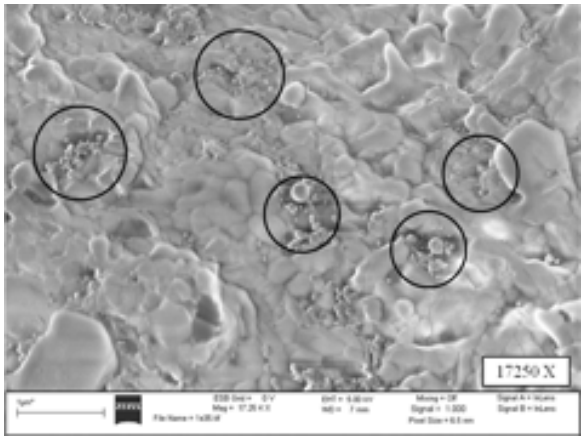

FIGURE 7: SEM images of the catalyst bed after flow shear testing [1].

ing the experimental data, by matching the exit hydrogen produced with the numerical results. For specified inlet flowrates, steam-to-methane ratio and net heat flux into the reactor, the α_s value was varied to match the bulk exit molar concentration for H_2 with the experiments. The bulk mass fraction (and concentration) at a cross-section is obtained as:

$$Y_{bulk,H_2} = \frac{1}{A_c \overline{u}} \int_{A_c} u Y_{H_2} dA. \tag{18}$$

where $\overline{u}$ is the average velocity at the cross-section of area A_c. The heat fluxes going into each section were not available, rather the total heat input into the reactor was obtained from experiments by doing an overall energy balance. The heat input was assumed uniformly distributed along the microchannel surface. Table 4 shows the different cases investigated and the corresponding reaction rate correction factors. Ideally, for all cases studied, the correction factor would remain constant; however,

as seen from the Table 4, some variation in α_s value is observed, showing a monotonous decrease with increase in net heat input to the reactor. Discarding the first two cases (as they indicate net negative heat input in the experimental data), and averaging the remaining α_s, the mean reaction rate correction factor was obtained to be 6.6×10^{-5}, indicating that the active catalyst sites were a small fraction, consistent with the visual observations in the SEM images. Once this averaged reaction-rate correction factor was determined, it was kept constant and all the cases were run again to establish the errors in numerically predicted exit hydrogen concentrations compared to experimental measurements. Table 5 indicates the errors in the predicted hydrogen concentrations compared to the experimentally measured values. Here, the dry concentrations (after removal of the steam for gas chromatography) are compared showing predictions with reasonable errors. Errors less than 16% were observed for all cases except one with low heat input. These errors are within the experimental uncertainty given considerable heat losses observed in the experimental facility [1].

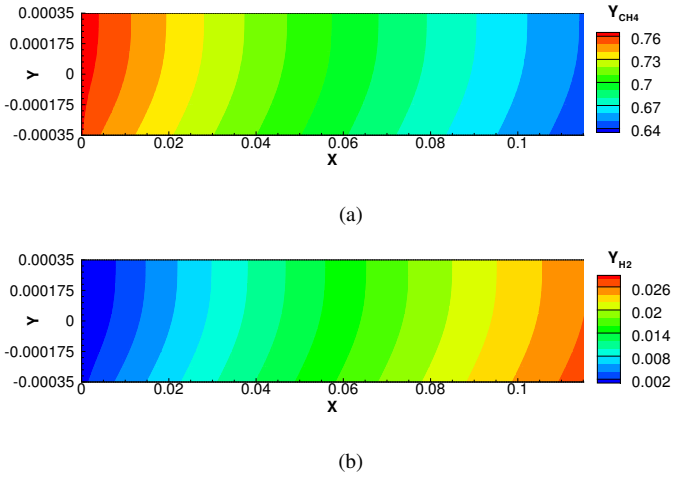

FIGURE 8: Steady state contours within the microchannel for a flow rate of 0.258 g/min: (a) CH_4 mass fraction, (b) H_2 mass fraction. Channel height is scaled up 100 times for clarity.

The chemical species generation and depletion along the channel length, the catalyst surface temperature, the catalyst surface reaction rates and net heats of reactions are difficult to measure with the experimental facility utilized in this work, but can be generated from the numerical model. Figure 8 gives the steady state contour plots for mass fractions of CH_4 and H_2 in the center plane of the channel for case C7 described in Table 4. Hot mixture of methane and steam enter the channel and conversion of methane to hydrogen begins near entrance. Owing to the strong endothermic reactions, the fluid-phase temperature near the bottom wall (catalyst region) decreases. It is observed that for the cases studied, only a small portion of methane is converted to hydrogen; which is consistent with the low number of activation sites for surface reactions.

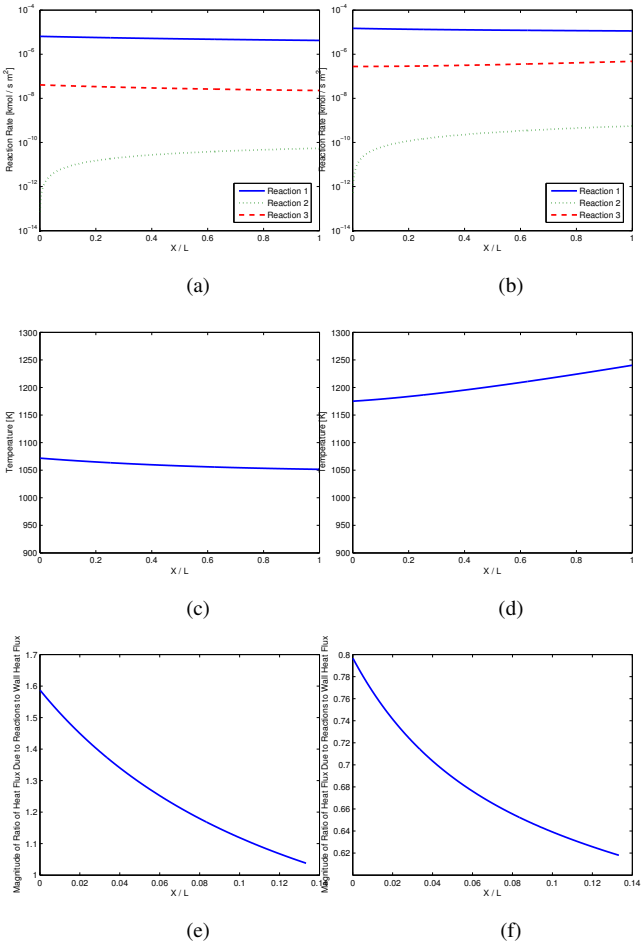

FIGURE 9: Steady state plots along the catalyst surface for cases C5 and C7 given in Table 4: (a,b) surface reaction rates for three chemical reactions, (c,d) surface temperature variations, (e,f) ratio of magnitudes of surface heat of reaction to input heat flux.

Figure 9a-f show the steady-state axial variations of catalyst surface reaction rates, temperatures, and ratio of magnitudes of heat of reaction to the heat flux input for two different cases studied C5 and C7. The inlet steam-to-methane ratio for both cases are around 3, and the methane flow rates are close to 0.19 g/min. The net heat flux for case C5 (840 W/m^2) is considerably lower than that for case C7 (3908 W/m^2). For both cases, it is observed that the reaction 1 is most dominant and has much higher reaction rates than the other two. The exothermic water-gas shift reaction

does play a role in production of CO and CO_2, however, its reaction rates are much smaller. It is also observed that the reaction rates for reaction 3 decreases along the channel for lower heat flux case (C5), whereas, it slightly increases for the higher heat flux case (C7). The surface temperature for case C5 decreases along the channel, whereas it increases for the higher heat flux case C7. Accordingly, the ratio of surface heat of reaction to the net heat flux is larger than 1 for case C5 and lower than 1 for case C7. This indicates that with increased heat input the reaction rates are generally higher and accordingly more hydrogen is produced as shown in Table 5. Since the rate of methane-to-steam conversion is higher in the initial stages of the channel, it indicates that maintaining high wall temperature at the inlet section may be beneficial for better conversion efficiency. For the cases studied, the methane conversion is not significant; however, can be enhanced by preparing the catalyst deposition in different ways. This was confirmed experimentally as shown by Eilers [1]. This work also indicates that proper characterization of the activation sites for microchannel catalyst deposition is essential. Use of a reaction rate correction factor for the reduced-reaction mechanisms, obtained from experimental measurements, can facilitate predictive modeling of methane-steam reforming in microchannel configurations.

Development of a one-dimensional model: To perform parametric studies varying inlet steam-to-methane ratio, inlet temperature, surface heat distribution, and net surface heat flux, full three-dimensional, reacting flow computations in the the entire flow geometry is feasible, but not practical. In order to reduce the time to solution in the numerical calculations of reacting flow and allow these parametric studies, a simplified one-dimensional reacting flow model for *steady state* solution was developed. Our main motivation here is to obtain a model that can be used for several parametric studies that can be used for optimizing the hydrogen production and designing the microchannel reactor. In addition, such a model can also be used to develop an optimized shape of a solar receiver that will provide a desired heat flux distribution along the length of the channel by combining the model with a Monte-Carlo radiative heat transfer solver, combining microchannel reaction simulation with conjugate heat transfer problem in the future.

Accordingly, the plane section of the microchannel (neglecting the inlet and outlet pipe sections in Figure 5c) was considered with one-dimensional grid along the flow direction. Using a simple staggered grid and neglecting diffusion in the wall-normal direction, the following steady state equations can be derived:

$$\frac{d}{dx}(\rho\overline{u}) = \frac{d}{dx}(\dot{m}'') = 0 \tag{19}$$

$$\frac{d}{dx}(\dot{m}''Y_i) = \frac{d}{dx}\left(\rho D\frac{dY_i}{dx}\right) + \dot{\omega}_i''' \tag{20}$$

$$\frac{d}{dx}(\dot{m}''C_p\frac{dT}{dx}) = \frac{d}{dx}\left(k\frac{dT}{dx}\right) + \dot{q}''', \tag{21}$$

where $\overline{u}$ is the average velocity over the cross-section of the microchannel, and $\dot{\omega}_i'''$ and $\dot{q}'''$ are source terms corresponding to the homogeneous gas-phase reactions in the species mass fraction and energy equations, respectively. In this work (as described before), the effect of gaseous-phase, homogeneous reactions was very small and these source terms are neglected. The majority of chemical conversion takes place on the catalyst surface giving rise to heterogeneous reactions modeled by the three surface reactions 1, 2, 3. Using a finite volume approach and integrating the one-dimensional model over the control volume, implementation of the surface reactions and surface heat flux into this model is fairly straight forward. The coupled equations for mass, species concentrations, and energy are solved using an iterative successive over-relaxation scheme. The species advection terms are discretized using a second-order Beam-Warming scheme, properties at the fluxes are evaluated using simple arithmetic averages, and diffusive fluxes are approximated using a piecewise linear profile assumption (resulting in a symmetric central differencing). Ideal gas law is used to compute density from temperature and a constant reactor pressure field (low-Mach number assumption). Solutions to this coupled system of equations is obtained within only a few seconds on a laptop.

In order to verify the one-dimensional model, case C7 was used. For simplicity, only one reaction (R1 1) was activated for this verification study. Comparison of the one-dimensional model and the full DNS study for this case are shown in Figure 10a,b. It is observed that the 1D model predicts the evolution of the hydrogen molar fraction as well as surface reaction rates very well. This also indicates that simple one-dimensional approximation to the governing equations as well as neglecting the inlet and outlet pipe sections has negligible effect overall results. The one-dimensional model is very efficient and thus useful for several parametric studies that can be used for optimization of hydrogen production.

CONCLUSION

Numerical experiments investigating effectiveness of a microchannel reactor geometry on methane-steam reforming are performed using a low-Mach number, variable density Navier-Stokes solver together with multicomponent reactions. Methane-steam reforming is modeled by three reduced-order reactions occurring on the reactor walls, two of which are endothermic re-

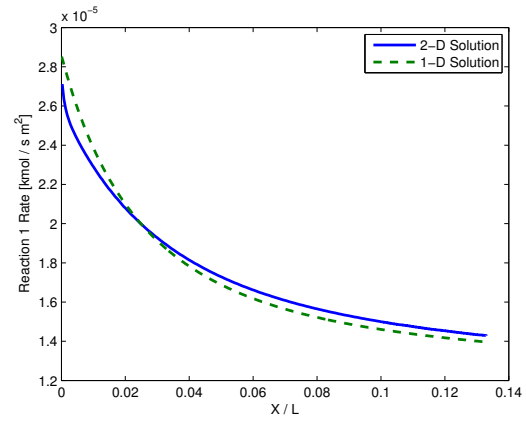

(a)

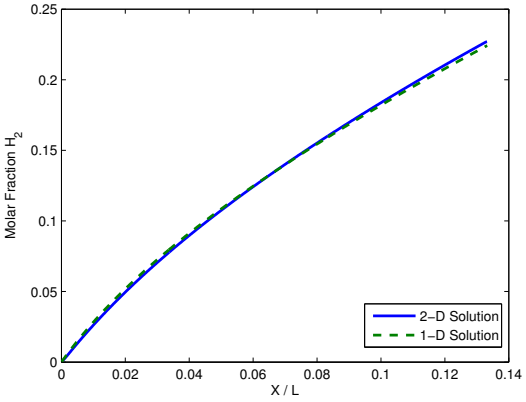

(b)

FIGURE 10: Comparison of one-dimensional model and full DNS study for case C7 with only one reaction (R1 1) activated. Axial variation of (a) H_2 molar fraction and (b) surface reaction rate are shown.

actions and an exothermic water-gas shift reaction. The surface chemical reactions are modeled as boundary conditions to the energy and species mass fraction equations, with Arrhenius-type reaction rate models for Palladium-deposited catalyst.

First the numerical approach was verified against experimental and numerical works on non-reacting flow in microchannels showing good predictive capability of the flow characteristics in high-aspect ratio channels. The approach was also used verify the validity of the Arrhenius-type reaction rate model for a Nickel catalyst, by comparing present predictions against the numerical work by Kuznetsov and Koslov [2] to show good agreement.

The validated numerical approach was then applied to predict hydrogen production in a microchannel setup based on the experimental setup of Eilers [1]. For these studies, the active Palladium catalyst sites were found to be few and distributed along the channel walls. In order to account for the non-uniformity and intermittency in active sites, a simple model modifying the reaction rate constant through a single constant factor was investigated. The reaction-rate correction factor was determined by matching the exit hydrogen production against the experimental data for one particular flow rate. Using this reaction-rate constant, simulations were performed at different flow rates and hydrogen production was compared with the experimental data to show reasonable agreement. This validation shows that use of an experimentally calibrated reaction-rate factor can be used to perform parametric studies and prediction of hydrogen production in microchannel reactors.

A simple one-dimensional model of the complex microchannel reactor was developed and verified against the resolved DNS study to show very good predictions. For the present cases studied, the thermo-diffusion effects (for example the Soret and Dufour effects) were not considered; however, it is conjectured that these effects may not affect the hydrogen production results significantly. Simulations are currently being performed varying the inlet steam-methane ratio, wall temperature distributions, and wall heat fluxes to investigate potential operating ranges for optimal production of hydrogen using microchannel configurations.

ACKNOWLEDGMENT

This work was funded partly by the Oregon Best Solar energy initiative and partly by US Army through the Oregon Nano and Microtechnology Institute (ONAMI). We also thank Prof. Murty Kanury of OSU for several useful discussions related to combustion and chemical kinetics modeling.

REFERENCES

[1] Eilers, B., 2010. "Microchannel steam-methane reforming under constant and variable surface temperature distributions". *M.S. Thesis, Oregon State University*.

[2] Kuznetsov, V., and Kozlov, S., 2008. "Modeling of methane steam reforming in a microchannel with a heat flow distributed in length". *Journal of Engineering Thermophysics,* ***17***(1), pp. 53–59.

[3] Wang, Y., Yoshiba, F., Kawase, M., and Watanabe, T., 2009. "Performance and effective kinetic models of methane steam reforming over Ni/YSZ anode of planar SOFC". *International Journal of Hydrogen Energy,* ***34***(9), pp. 3885–3893.

[4] Xu, J., and Froment, G., 1989. "Methane steam reforming, methanation and water-gas shift: I. Intrinsic kinetics". *AIChE Journal,* ***35***(1), pp. 88–103.

[5] Hou, K., and Hughes, R., 2001. "The kinetics of methane steam reforming over a Ni/α-Al2O catalyst". *Chemical Engineering Journal,* ***82***(1-3), pp. 311–328.

[6] Deutschmann, O., and Schmidt, L., 1998. "Modeling the partial oxidation of methane in a short-contact-time reactor". *AIChE Journal,* ***44***(11), pp. 2465–2477.

[7] Appel, C., Mantzaras, J., Schaeren, R., Bombach, R., Inauen, A., Tylli, N., Wolf, M., Griffin, T., Winkler, D., and Carroni, R., 2005. "Partial catalytic oxidation of methane to synthesis gas over rhodium: in situ raman experiments and detailed simulations". *Proceedings of the Combustion Institute,* ***30***(2), pp. 2509 – 2517.

[8] Bird, R., Stewart, W., and Lightfoot, E. "Transport Phenomena, Wiley, New York, 1960".

[9] Stutz, M. J., and Poulikakos, D., 2005. "Effects of microreactor wall heat conduction on the reforming process of methane". *Chemical Engineering Science,* ***60***(24), pp. 6983 – 6997.

[10] Kenneth, K., 2005. "Principles of combustion". *John Wiley's sons, Ine, Hoboken, New Jersey*.

[11] Turns, S., 1995. "An introduction to combustion: Concepts and applications(Book)". *New York: McGraw-Hill, Inc, 1995*.

[12] Shu, J., Grandjean, B., and Kaliaguine, S., 1994. "Methane Steam Reforming in Asymmetric Pd-Ag and Pd-Ag/Porous SS Membrane Reactors". *Applied Catalysis A: General,* ***119***(2), pp. 305–325.

[13] Moin, P., and Apte, S., 2006. "Large-eddy simulation of realistic gas turbine combustors". *AIAA Journal,* ***44***(4), pp. 698–708.

[14] Apte, S., Mahesh, K., Moin, P., and Oefelein, J., 2003. "Large-eddy simulation of swirling particle-laden flows in a coaxial-jet combustor". *International Journal of Multiphase Flow,* ***29***(8), pp. 1311–1331.

[15] Mahesh, K., Constantinescu, G., Apte, S., Iaccarino, G., Ham, F., and Moin, P., 2006. "Large-eddy simulation of reacting turbulent flows in complex geometries". *Journal of Applied Mechanics,* ***73***, p. 374.

[16] Ham, F., Apte, S., Iaccarino, G., Wu, X., Herrmann, M., Constantinescu, G., Mahesh, K., and Moin, P., 2003. "Unstructured LES of reacting multiphase flows in realistic gas turbine combustors. Annual Research Briefs 2003". *Center for Turbulence Research, NASA Ames/Stanford Univ*, pp. 139–160.

[17] Qu, W., Mudawar, I., Lee, S., and Wereley, S., 2006. "Experimental and computational investigation of flow development and pressure drop in a rectangular micro-channel". *Journal of Electronic Packaging,* ***128***, p. 1.